

1 Assessment of the position accuracy of a single-frequency GPS 2 receiver designed for electromagnetic induction surveys

3 Sebastian Rudolph^{1,2*}, Ben Paul Marchant³, Lutz Weihermüller¹ and Harry Vereecken¹

4 ¹ Forschungszentrum Jülich GmbH, Agrosphere Institute (IBG-3), Jülich, Germany

5 (sebastian.rudolph@julumni.fz-juelich.de)

6 ² Thünen Institute of Rural Studies, Braunschweig, Germany

7 ³ British Geological Survey, Environmental Science Centre, Keyworth, England

8 * Correspondence: sebastian.rudolph@julumni.fz-juelich.de; Tel.: +49-2461-61-8669

9
10
11
12
13 Acknowledgments: This study was supported by the Federal Ministry of Education and Research
14 (Competence network for phenotyping science-CROP.SENSE.net). The contributions of B.P.
15 Marchant are published with the permission of the Executive Director of the British Geological
16 Survey (NERC).

17
18 **Abstract:** In precision agriculture (PA), compact and lightweight electromagnetic induction (EMI) sensors
19 have extensively been used to investigate the spatial variability of soil, to evaluate crop performance, and to
20 identify management zones by mapping soil apparent electrical conductivity (ECa), a surrogate for primary
21 and functional soil properties. As reported in the literature, differential global positioning systems (DGPS)
22 with sub-metre to centimetre accuracy have been almost exclusively used to geo-reference these
23 measurements. However, with the ongoing improvements in Global Navigation Satellite System (GNSS)
24 technology, a single state-of-the-art DGPS receiver is likely to be more expensive than the geophysical sensor
25 itself. In addition, survey costs quickly multiply if advanced real time kinematic (RTK) correction or a base
26 and rover configuration is used. However, the need for centimetre accuracy for surveys supporting PA is
27 questionable as most PA applications are concerned with soil properties at scales above 1 m. The motivation
28 for this study was to assess the position accuracy of a GNSS receiver especially designed for electromagnetic
29 induction surveys supporting PA applications. Results show that a robust, low-cost and single-frequency
30 receiver is sufficient to geo-reference ECa measurements at the within-field scale. However, ECa data from a
31 field characterized by a high spatial variability of subsurface properties compared to repeated ECa survey
32 maps and remotely sensed leaf area index (LAI) indicate that a lack of positioning accuracy can constrain the
33 interpretability of such measurements. It is therefore demonstrated how relative and absolute positioning errors
34 can be quantified and corrected. Finally, a summary of practical implications and considerations for the geo-
35 referencing of ECa data using GNSS sensors are presented.

36 **Keywords:** Single-frequency GPS receiver; GNSS position accuracy, Electromagnetic induction (EMI)
37 survey; ECa

39 **Introduction**

40 Precision agriculture (PA) is a crop management strategy, which aims to optimise field-level management
41 with regard to crop farming, environmental protection, and economics. To understand the field-scale variability
42 of crop status and environmental state properties new technologies such as airborne and satellite remote sensing,
43 satellite based navigation systems, and geographical information systems (GIS) are being used (Bramley 2009).
44 To minimise cost and effort of conventional point-by-point characterization of soil properties, mobile
45 geophysical sensors, which can provide direct or indirect measurements of specific soil properties, have
46 intensively been used in the last decade (Sudduth et al. 2001; Corwin 2008). Electromagnetic induction (EMI)
47 measures soil apparent conductivity (ECa) by emitting an electromagnetic field while the response from the
48 conductive subsurface is recorded. EMI instruments are the most commonly used geophysical sensors in PA
49 and have been extensively used to investigate the spatial variability of soil, to estimate soil water content, clay
50 content, soil depth, nutrient status, and also to evaluate crop performance, to identify crop management zones
51 and to support agricultural experimentation (Eigenberg and Nienaber 2003; Jaynes et al. 1995; Kachanoski et
52 al. 1988; Triantafilis and Lesch 2005; Frogbrook and Oliver 2007; Rudolph et al. 2016; Corwin 2008).

53 Commonly, EMI derived measurements are geo-referenced using a Global Navigation Satellite System
54 (GNSS) such as the American Global Position System (GPS), the Chinese BeiDou Navigation Satellite System
55 (BDS) or the Russian Global Navigation Satellite System (GLONASS). Using the GPS as an example, complex
56 signals containing the precise time and orbital information are broadcasted by GNSS satellites in the form of
57 the Coarse Acquisition Code (C/A code with 1.023 MHz), the Precise Code (P code with 10.23 MHz), and the
58 navigation message (50 Hz) to the earth using different carrier frequencies in the L-band (1-2 GHz)(Kaplan and
59 Hegarty 2006).

60 The GNSS receiver decodes respective information and calculates its geo-position based on the principles
61 of triangulation. However, GNSS positioning accuracy is mainly constrained by satellite geometry, which
62 describes the position of satellites relative to each other from the view of the receiver, atmospheric delay, a
63 frequency dependent delay of the satellite signals passing through the troposphere and ionosphere, as well as
64 multipath effects, caused by signal reflection from secondary sources (Leick et al. 2015).

65 In general, GNSS receivers can be distinguished based on the number of frequencies the sensor is capable
66 of receiving (e.g. single-frequency (L1), multi-frequency systems (L1, L2, L5)), the concurrent reception of
67 GNSS providers (e.g. single-constellation (GPS), multi-constellation (GPS/ GLONASS/BeiDou)), and whether
68 code only or code and carrier-phase observations are used by the receiver (El-Rabbany 2006).

69 The advantages of the multi-frequency, multi-constellation systems are obvious. Atmospheric delay,
70 multipath and receiver noise can be corrected by the concurrent reception of multiple frequencies, while
71 balanced satellite geometry is more likely when information is received from as many satellites as possible.
72 Furthermore, the navigation accuracy of the GNSS receiver considerably improves when pseudorange
73 measurements, the distance between GNSS satellite and receiver, are obtained from the higher-resolution
74 carrier-phase observations (wavelength 0.19 m) than from the code observations (wavelength 300 m) instead
75 (Kaplan and Hegarty 2006). Moreover, real-time kinematic (RTK), which relies on differential carrier-phase
76 observations, received by radio modems from either a nearby reference station or GSM (Global System for
77 Mobile Communications), enables sub-centimeter levels of positioning.-These benefits have led the Australian
78 Grains Research and Development Corporation to recommend differential GPS (DGPS) as the minimum level
79 of accuracy for EMI surveys (O'Leary 2006).

80 However, modern geodetic-grade GNSS systems with centimetre accuracy are costly. Weltzien et al.
81 (2003) reported an exponential relationship between GNSS accuracy and acquisition cost. At present, the costs
82 for a fully operable multi-frequency, multi-constellation GNSS unit for commercial purpose starts above 15,000
83 € (personal communication Leica). In areas with insufficient GSM coverage an additional GNSS unit might
84 have to be purchased to enable RTK correction. However, despite all possible upgrades a robust positioning
85 performance cannot be guaranteed and the possible loss of the correction signal will inevitably cause artefacts
86 in the positioning. Such erroneous survey observations have then either to be removed (Delefortrie et al. 2014)
87 or corrected using post processing software (Kaplan and Hegarty 2006).

88 In contrast, a single-frequency GNSS receiver for less than 500 € might not be as accurate, but if the
89 positioning accuracy of the receiver satisfies the demands of the proposed survey why should the surveyor not
90 use a simpler GNSS unit? Beside acquisition costs, the requirement of a DGPS for ECa surveying is
91 questionable as PA applications are generally concerned with soil properties measured on a scale above 1 m
92 (McBratney and Pringle 1999) and most PA equipment only requires positioning with sub 3 m accuracy
93 (McCloud et al. 2007). Furthermore, as most of the optical satellite imagery used in PA is sensed with a
94 resolution of 5 x 5 m or above McBratney et al. (2003) proposed a pixel resolution of 5 x 5 m for proximal
95 sensed high resolution soil survey maps.

96 Despite these arguments only a few published EMI studies have relied on a single-frequency GNSS
97 receiver. For example, Francés and Lubczynski (2011) used a standard GPS receiver with a horizontal accuracy
98 of ± 2.5 m to reference EM-31 measurements, which they found to be satisfactory considering the scale of the
99 spatial variation of surveyed clayey topsoil thickness. Similar GNSS systems were used by Vitharana et al.
100 (2008), Mertens et al. (2008), López-Lozano et al. (2010), and Huang et al. (2014) to geo-reference ECa
101 measurement taken in agricultural fields.

102 However, none of these studies highlighted accuracy-related issues for the interpretability of the resulting
103 measurements. Furthermore, although the GNSS units utilised were optimised for good and stable navigation
104 performance, the handheld receivers were designed for adventure outdoor activities and not to support
105 geophysical surveys. Therefore, an affordable, robust and compact, easy to operate GNSS unit is needed for
106 ECa survey supporting PA applications.

107 The objectives of this study were: i) to design an inexpensive L1 GNSS receiver for EMI surveys, ii) to
108 quantify its position accuracy relative to an RTK-DGPS using static and dynamic measurements, iii) to
109 quantify and correct positioning errors using repeated ECa measurements and secondary data.

110 **Materials and Methods**

111 *The L1 GNSS system*

112 The GNSS unit described here (expressed as EMI-GPS hereafter, see Figure 1) was designed to meet the
113 needs of electromagnetic prospection surveys. Hardware components costing around 400 € were integrated into
114 a compact (200x10x10 mm), robust, and waterproofed plastic housing. The core of the EMI-GPS is an Ublox
115 LEA-6T (Thalwil, Switzerland) GPS. The single-frequency (L1 C/A code) GPS receiver operates with a
116 maximal navigation update rate of 2 Hz and has a horizontal accuracy of 2.0 m with activated satellite-based
117 augmentation system (SBAS) which accounts for satellite orbit and clock errors as well as atmospheric delay
118 (Ublox 2010; Kaplan and Hegarty 2006). A compact Novatel ANT-537 L1 GPS patch antenna mounted on top
119 of the plastic housing is used to receive GPS information. Position information in the form of the NMEA

120 (National Marine Electronics Association)(National Marine Electronics Association 2012) and the Ublox RAW
121 format can either be recorded on an internal 2 GB SD-card or transmitted via an RS232 port to the geophysical
122 sensor. The same port can be used to configure the module by Ublox u-center a freely available GNSS
123 evaluation software(Ublox 2016), which allows the user to change between GNSS settings for different EMI
124 sensors. The electronics of the EMI-GPS is powered by four easily replaceable AA Mignon Ni-MH
125 rechargeable batteries, which last in operation for more than 12 h. Beside the low-cost and low-power
126 consumption of the Ublox LEA-6T GPS module, the form factor ensures an easy upgrade to future Ublox LEA
127 modules. Furthermore, the recorded RAW messages can be used by RTKLIB, a widely used, powerful, and
128 highly portable open source software for real-time and post processing of GNSS data (Takasu and Yasuda
129 2009).
130



131
132 **Figure 1.** Electronic and hardware components of the EMI-GPS system depicted without the waterproofed plastic housing
133 and GNSS antenna.

134 *Assessment of the relative accuracy of the EMI-GPS determined by stationary recording*

135 The most important parameter for validating GNSS receivers is the accuracy of positioning. This
136 parameter is commonly assessed by the manufacturer based on static experiments in which the sensor is held
137 fixed at a known location for a long time period (Taylor et al. 2004). However, since GNSS accuracy is subject
138 to much marketing terminology, the accuracy should always be quantified under real operating conditions.

139 Therefore, a static performance test over 6 h was carried out at the TERENO test site Rollesbroich (Bogena
140 et al. 2016). The site (50°37'33"N 6°18'19"E) is located 50 km west of Bonn (Germany) and is ideal for
141 evaluating the GNSS receiver due to the absence of trees, buildings, and other tall objects. However, due to the
142 remoteness of the area, the establishment of a stable RTK connection for correcting DGPS observations is
143 challenging and for most of the time not possible. During the experiment, the EMI-GPS was placed on the
144 ground and NMEA-GGA messages were recorded at 2 Hz to the internal SD-card.

145 The 2D accuracy of the receiver was quantified by calculating the Circular Error Probability (CEP), the
146 Distance Root Mean Square parameter (DRMS), and two times this value, which is referred to as 2DRMS by
147 Kaplan and Hegarty (2006). Each accuracy measure defines a radius from the true location describing a
148 confidence region in which observations can be expected with a specific probability. The CEP is derived directly
149 from the position error distribution and refers to the radius of a circle in which 50 % of the GNSS observations
150 are measured. The CEP is calculated as:

$$CEP = 0.62 \delta_y + 0.56 \delta_x, \quad (1)$$

151 where δ_x and δ_y are the standard deviations of the longitudinal and latitudinal coordinates, respectively
 152 (NovAtel Inc. 2003). The DRMS defines a region in which 63-68 % of the observations are made and is
 153 calculated as:

$$DRMS = \sqrt{\delta_x^2 + \delta_y^2}. \quad (2)$$

154 The 2DRMS instead defines the area containing 95-98 % of the observations and is calculated as:

$$2DRMS = 2\sqrt{\delta_x^2 + \delta_y^2}. \quad (3)$$

155 As the true location of the EMI-GPS could not be determined by a DGPS the median of all observations
 156 was used as a reference point. For the analysis, coordinates had to be transformed from the global WGS84 into
 157 the metric UTM32 system and were then standardised on the reference coordinates. The dispersion of the
 158 horizontal error, calculated as the shortest distance between observations and the reference was then compared
 159 against the theoretical horizontal error distribution. The theoretical horizontal error function was derived from
 160 a Weibull distribution with scale parameter $\alpha=1$ and shape parameter $\beta=2$ which is commonly used to model
 161 radial navigation errors (Kobayashi et al. 1992).

162 To further quantify the EMI-GPS measurements the position fix status, the number of satellites, as well as
 163 the Horizontal Dilution of Precision (HDOP) as provided by the NMEA-GGA messages, were analysed.

164 *Assessment of the absolute accuracy of the EMI-GPS determined in a kinematic experiment*

165 In addition to the stationary positioning, Taylor et al. (2004) noted that the reported accuracy of a GNSS
 166 receiver can vary significantly in dynamic mode. The position accuracy of two EMI-GPS receivers (expressed
 167 as Rover01 and Rover02 hereafter) was therefore compared against a NovaTel ProPak-V3 L1/L2 DGPS
 168 (NovAtel Inc., Calgary, Canada) with GSM-RTK correction in a kinematic experiment. Respective GNSS
 169 antennas were mounted at the same height and separated by 0.2 m with the DGPS antenna at central position
 170 on a test cart (see Fig. 3a), which was pulled at walking speed along the side markings of a road. Neither
 171 buildings nor other nearby obstacles affected the measurements. All GNSS observations were recorded as
 172 NMEA-GGA message with 1 Hz to the internal memory.

173 The robustness of the Rover observations were assessed by the following procedure. First, the closest
 174 DGPS location was determined for each Rover observation considering the recorded GPS time. Then, the
 175 direction of travel was reconstructed by fitting a smooth line through the six closest DGPS observations.
 176 Subsequently, the selected Rover observations were rotated around the DGPS reference location so that the
 177 direction of travel was pointing against north.

178 Under the assumption that the EMI-GPS would have recorded with almost perfect accuracy one should
 179 assume that the rotated Rover observations would cluster around a distinct position separated by 0.2 m from the
 180 origin, representing the DGPS reference location. Furthermore, the error distribution in longitudinal and
 181 latitudinal direction would be symmetric with its highest frequency at the centre. In contrast, a clustering further
 182 away from the reference as well as a distinct deviation from a circular pattern will indicate possible position
 183 errors, which can be described by descriptive statistics or the above-mentioned accuracy measures.

185 *Quantification of the relative and absolute position accuracy of the EMI-GPS using ECa survey data and*
186 *secondary data*

187 In non-saline soils the spatial variation of ECa is primarily a function of soil texture, moisture content, and
188 cation exchange capacity. Sudduth et al. (2001) showed that ECa patterns are spatially and temporally stable if
189 the contribution of soil texture, especially clay content, dominates all other factors. Furthermore, a strong
190 collinearity between shallow and deep ECa measurements can be expected. Recently, Rudolph et al. (2015)
191 demonstrated that time variable crop-status patterns observed by multispectral satellite imagery can be linked
192 to temporally stable ECa patterns. Hence, the relative positioning error of the EMI-GPS can be determined
193 using repeatedly measured ECa data, while the absolute error can be assessed by using remotely sensed crop
194 status measurements as reference. To quantify the relative and absolute positioning error ECa data of the
195 TERENO site Selhausen - field F01 – from 2012 as well as an unpublished ECa dataset of the same field
196 obtained in 2015 are considered. For both surveys, ECa data were obtained by the CMD miniExplorer
197 (GFInstruments, Brno, Czech Republic) and measurements were geo-referenced by the above mentioned EMI-
198 GPS. The EMI sensor consists of three receiver coils separated by $d_1 = 0.32$, $d_2 = 0.71$, and $d_3 = 1.18$ m from the
199 transmitter coil. The resulting theoretical exploration depth for the vertical coplanar (VCP) mode ranges from
200 0 - 0.25 m (VCP1), 0 - 0.5 m (VCP2) and 0 - 0.9 m (VCP3) and for the horizontal coplanar (HCP) mode from
201 0 - 0.5 m (HCP1), 0 - 1.1 m (HCP2) and 0 - 1.9 m (HCP3), respectively. Due to the measurement principles of
202 the EMI sensor, VCP and HCP data had to be obtained separately. For the published ECa survey VCP and HCP
203 measurements were taken on two consecutive days, while for the later survey a second CMD miniExplorer was
204 used to measure VCP and HCP simultaneously. In the so-called tandem-approach, both EMI sensors were
205 pulled behind each other and geo-referenced separately. At any time the EMI-GPS was mounted in the center
206 and 1.5 m above the EMI sensor while GNSS observations were transmitted to the ECa logger by 0.5 Hz. A
207 detailed measurement setup is given by Rudolph et al. (2015).

208 Maps of the log-transformed and variance normalised ECa data were produced using geostatistical
209 methods (Webster and Oliver 2007). A spatial autocorrelation amongst the data was represented by a Matérn
210 variogram function (Minasny and McBratney 2005; Matérn 1986):

$$\gamma(h) = c_0 + c_1 \left(1 - \frac{1}{2^{\nu-1}\Gamma(\nu)} \left(\frac{h}{a}\right)^{\nu} K_{\nu}\left(\frac{h}{a}\right) \right) \text{ for } h > 0 \text{ and } \gamma(0) = 0, \quad (4)$$

211 where h is the lag distance separating two observations, c_0 is the nugget variance describing the positive
212 intercept on the ordinate for zero lag distance, and c_0+c_1 describe the sill variance of the variogram which equals
213 the variance of the underlying population. Γ is the gamma function, K_{ν} denotes the modified Bessel
214 function of the second kind, while $\nu > 0$ and $a > 0$ are smoothness and scale parameters, respectively. These
215 parameters were estimated by the method of moments and then used to interpolate the ECa measurements to a
216 raster with 0.25 m resolution using ordinary kriging (Webster and Oliver 2007).

217 For both ECa surveys, the relative position accuracy was assessed as follows. Within a search radius of 10
218 m, the interpolated VCP measurements were shifted stepwise in increments of 0.25 m relative to the HCP data.
219 For each step, the Pearson correlation coefficient (r) was calculated between the position-corrected VCP and
220 the measured HCP raster combinations (e.g. VCP1-HCP1, VCP1-HCP2, VCP1-HCP3). Respectively, the sum
221 of all correlation coefficients was computed to quantify the positioning error. Assuming a strong collinearity
222 between shallow VCP and deep HCP data, the relative position error would be indicated by the largest sum of

223 all correlation coefficients. Once the error is obtained, the position of the VCP measurements can be corrected
224 by applying the determined displacement vector.

225 In contrast, the absolute position accuracy was quantified similarly, but the interpolated VCP and HCP
226 measurements were shifted and correlated against geo-referenced leaf area index measurements (LAI).
227 Respective crop canopy measurements were taken in 2011 and are described by Rudolph et al. (2015). One
228 should note, that larger observed LAI values indicated better crop performance under dry conditions due to a
229 higher water holding capacity of the soil. As the water holding capacity is a function of clay content, similar
230 patterns were described by the ECa survey. Zones of better crop performance were delineated manually in the
231 western part of the field by a DGPS in 2013 as another severe drought period affected sugar beet. To evaluate
232 the correction of the absolute error these delineated zones were visually compared with the measured and
233 position corrected ECa data using a GIS. Furthermore, position-corrected ECa data were regressed with soil
234 texture information as described by Rudolph et al. (2015) and the coefficients of determination (R^2) obtained
235 were compared against the values derived from the measured ECa data.

236 **Results and discussion**

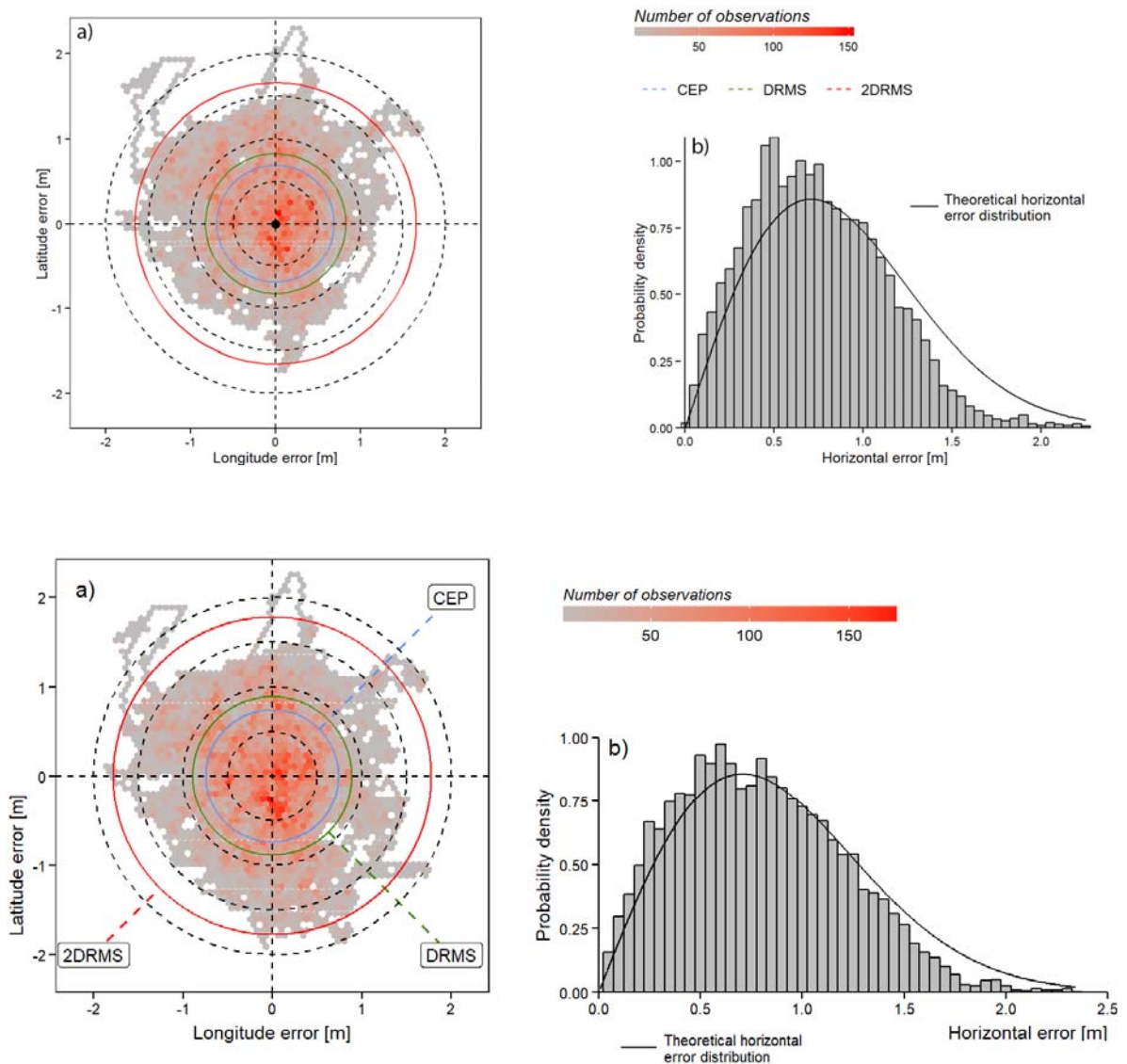
237 *Relative accuracy of the EMI-GPS determined by the static performance test*

238 Satellite visibility during the static performance test was good and the number of tracked satellites ranged
239 from 8 to 12 with a median of 10. The high number of visible satellites resulted in an ideal satellite geometry
240 as indicated by the HDOP, which varied between 0.75 and 1.2. A median HDOP of 0.8 indicated a very good
241 satellite constellation (Kaplan and Hegarty 2006). The analysis of the position fix status information revealed
242 that the first 51 observations were recorded without SBAS correction. The missing correction can be explained
243 by the start mode of the receiver as well as the fact that the EMI-GPS is designed to record or transmit NMEA
244 messages as soon as the receiver is switched on. In general, three start modes can be distinguished depending
245 on the available GNSS information. If the receiver has no prior information about its current position, for
246 example if the receiver was switched off for a longer time period and has been moved to another location, then
247 information such as satellite constellation and UTC time have to be obtained before the new position can be
248 determined. Hence, the so-called cold start is slower than the warm or hot start. As the EMI-GPS was set up to
249 record its position at 2 Hz, the first 26 s were affected by the missing correction. The same time period is given
250 by the manufacturer of the LEA-6T GPS module for the cold start (Ublox 2010). Although, this time period is
251 insignificant for a continuous EMI survey, warm up times should always be considered, especially for surveys
252 at which the GNSS receiver is frequently switched on and off such as for a manual grid survey covering several
253 hectares.

254 As summarised in Figure 2a, the recorded observations scatter within a radius of 2.3 m around the
255 reference (median of all positions). The deviation from the reference was on average 0.76 m with a standard
256 deviation of 0.41 m. CEP, DRMS and 2DRMS indicate that 50 % of the observations were made within 0.7 m,
257 68 % within 0.9 m and 98 % within 1.8 m. However, one should consider that in the reported experiment the
258 system precision was accessed using the median of all measurements as a reference and that this approximation
259 to the actual position contains a bias that will affect the results. Furthermore, as illustrated in Figure 2b the
260 comparison between the measured and theoretical error distribution indicates a high frequency of small errors
261 and a low frequency of larger errors. Since the comparison indicates that the horizontal measurement error was
262 not entirely circular distributed nor Gaussian, the estimated CEP, DRMS and 2SDRMS values are likely to be

263 underestimated due to the short observation time. In contrast, UBLOX quantifies the horizontal position
 264 accuracy of the LEA-6T module at 2 m based on the CEP and a 24 h static performance test (Ublox 2010). Due
 265 to practical reasons, a longer observation time was not possible.

266
 267



268

269 **Figure 2.** EMI-GPS observations of a 6 h static performance test. The scattering of all observations around its median
 270 quantified on the number of observations per area is illustrated in a) together with the Circular Error Probability (CEP), the
 271 Distance Root Mean square parameter (DRMS), and its double value the 2DRMS, which quantify the 2D accuracy of the
 272 EMI-GPS receiver during this experiment. In b) the dispersion of the observed horizontal error is compared against the
 273 theoretical horizontal error distribution derived from a Weibull distribution with scale parameter $\alpha=1$ and shape parameter
 274 $\beta=2$.

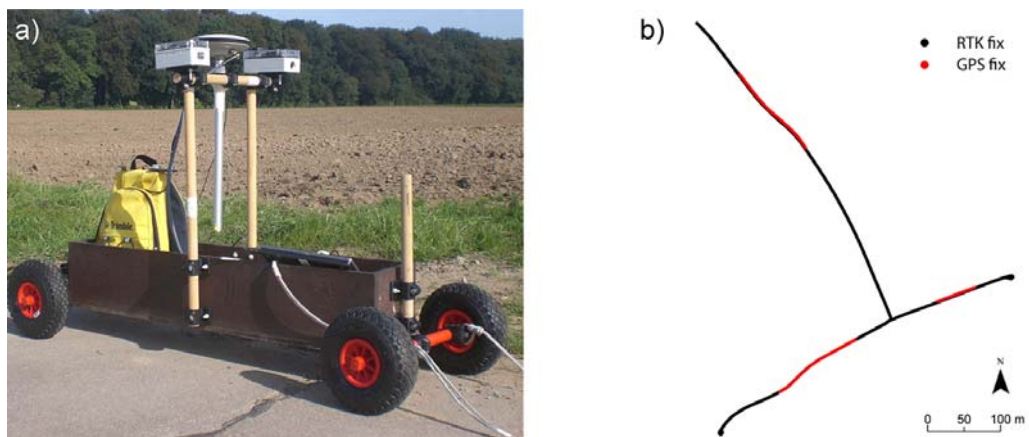
275 *Positioning accuracy of the EMI-GPS when operated in dynamic mode*

276 During the kinematic experiment, satellite geometry was good as indicated by HDOP values which ranged
 277 for both Rover and the DGPS between 0.9 and 1.4. Larger differences were observed in the number of satellites
 278 used for position calculation. While the DGPS acquired on average seven satellites three more were used by the
 279 Rovers. These differences can possibly be explained by the antennas used as well as differences in the
 280 acquisition settings. For example, the elevation cut-off angle is a predefined parameter, which ensures that only
 281 satellites with a certain angle above the horizon are used by the receiver for position calculation. Although, a

282 low cut-off angle generally results in a larger number of satellites it also increases the possibility of tropospheric
 283 or ionospheric delay, multipath errors, or blockage of the line-of-sight. In contrast, a high cut-off angle might
 284 exclude potential satellites and negatively affect the satellite constellation in view of the GNSS receiver. For
 285 the reported EMI-GPS measurements the default cut-off angle of 5° was used, whereas the angle used by the
 286 DGPS was unknown.

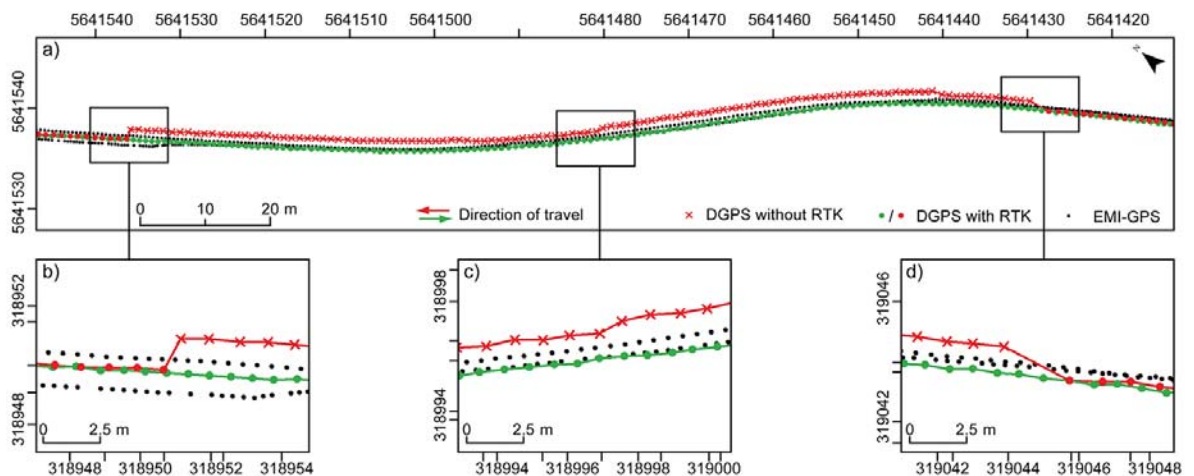
287 The analysis of the DGPS logs revealed that RTK correction had unnoticeably been lost three times during
 288 the data gathering and it took up to 2.5 minutes to re-establish the respective corrections (see Figure 3b). The
 289 RTK loss is illustrated in Figure 4 by comparing DGPS and Rover02 logs recorded along a 165 m long transect.
 290 As part of the 2.3 km long experimental track, the section was traversed twice. While DGPS observations logged
 291 with 1 Hz were in accordance with the road markings during the first pass a sudden jump and a varying offset
 292 of up to 2 m towards east indicates the loss of the RTK correction on the return (see Figure 4c and d). As soon
 293 as RTK-connection was re-established, DGPS recordings align perfectly as visualised in Figure 3b. In contrast,
 294 observations of Rover02 logged at 2 Hz showed no erratic behaviour at all but follow the reference track with
 295 a varying offset. However, the quantified position offset was at no time larger than for those of the DGPS
 296 without RTK correction.

297



298

299 **Figure 3.** The experimental cart with the two EMI-GPS Rovers (Rover01 and Rover02) and the RTK corrected DGPS are
 300 depicted in a) while the layout of the test track colour-coded by the NMEA 0183 GPS quality indicator (National Marine
 301 Electronics Association 2012) is illustrated in b).



302

303

304 **Figure 4.** Comparison between the EMI-GPS and the DGPS observations along a 200 m long transect in the northern part
 305 of the experimental track. The loss of the RTK correction on the return (red colour) is illustrated in a). The sudden loss of
 306 respective correction is depicted in d) illustrated by the large offset in the DGPS observations. Subfigure c) and d) indicate
 307 that the EMI-GPS observations made in both directions are more similar than those made for the DGPS without RTK. The
 308 re-establishment of the RTK correction is illustrated in b).

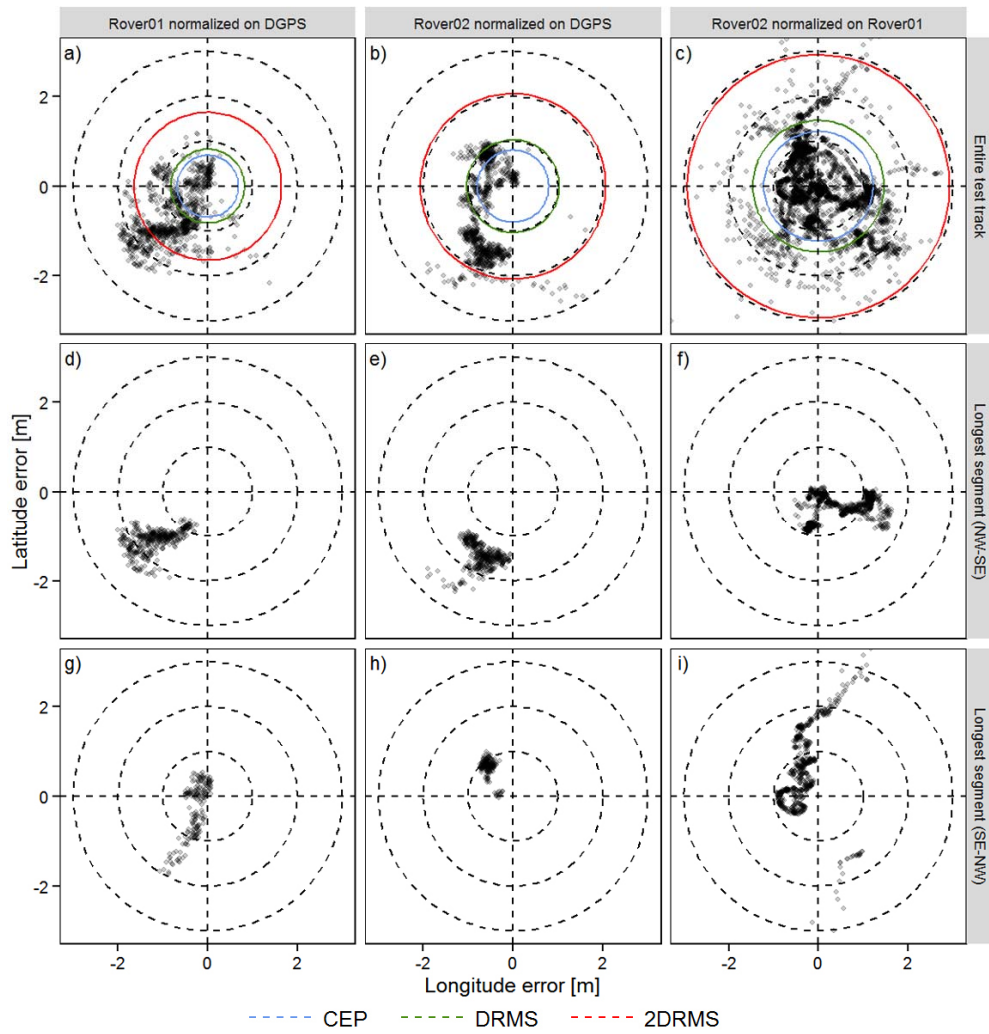
309 The comparison of the EMI-GPS observation acquired in the kinematic and static experiment suggests
 310 that a kinematic filter algorithm is used by the LEA-6T GPS module as indicated by the good in-line alignment
 311 of respective observations. This assumption is strengthened by the fact that observations of both Rovers drifted
 312 away from the reference by up to 1.2 m as the cart stopped for 30 s (data not shown). However, the use of a
 313 filter, which smooths the signal to noise ratio as suggested in the literature, could not be verified by the
 314 information provided by the manufacturer (Ehrl et al. 2003).

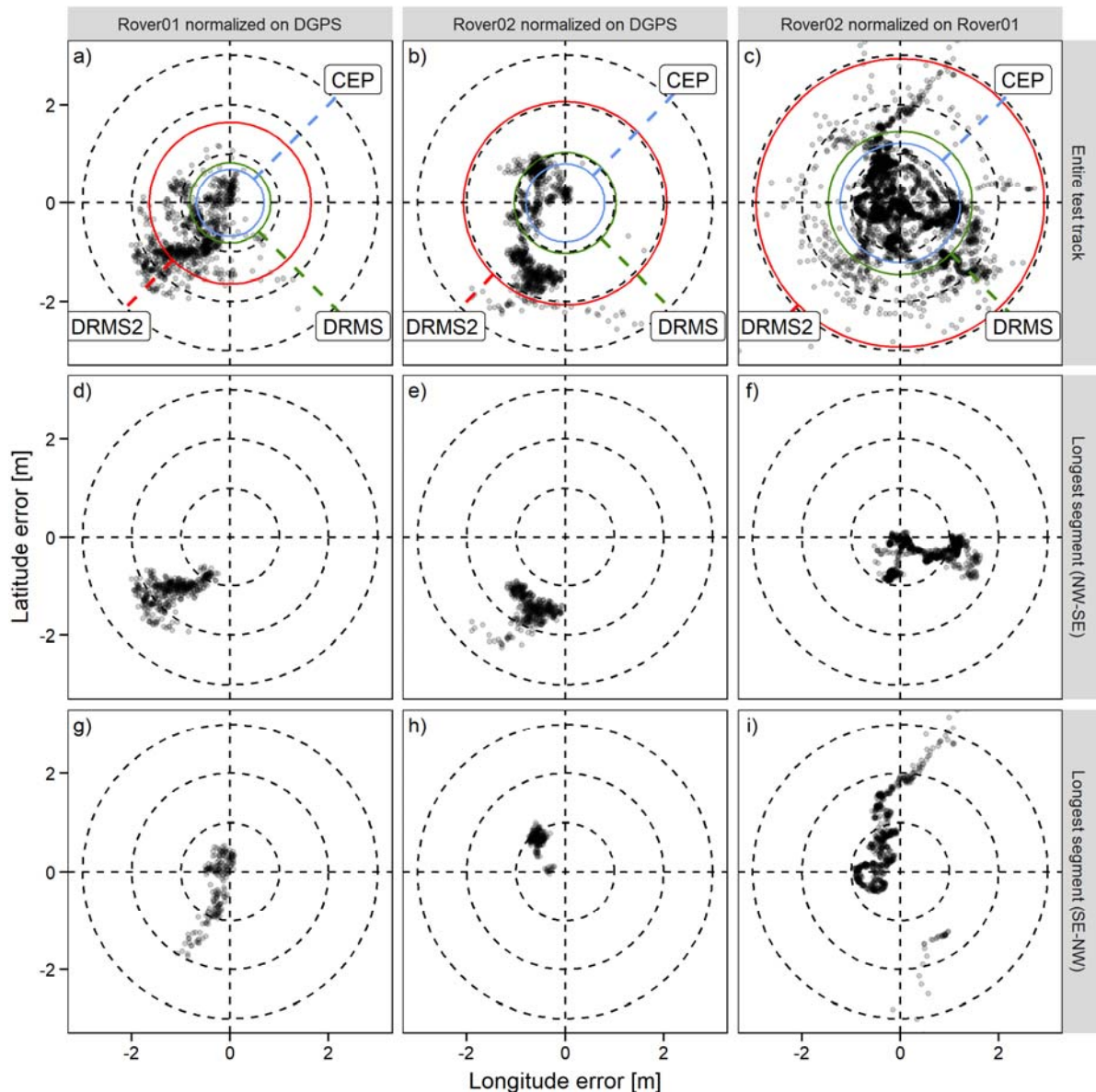
315 The comparison between the DGPS reference and the rotated and normalised Rover observations are
 316 summarized in Table 1 and depicted in Figure 5a and b. Please note that DGPS observations recorded without
 317 RTK correction were removed previously. Although, Rover observations scattered within 2.5 m around the
 318 reference location, the scattering appeared to be unbalanced and more localised than compared to the static
 319 performance test. The high number of observations in the 3rd and 4th quadrant of the Cartesian coordinate
 320 system can partly be explained by the layout of the experiment as the majority of the observations were made
 321 along tracks in NW-SE (41 %) and SE-NW (23 %) directions. Furthermore, problems with the RTK correction
 322 occurred predominantly along the shorter NE-SW, and SW-NE segments of the track (see Figure 3b).

323 **Table 1.** Error quantification of the EMI-GPS observations referenced on a DGPS and obtained during the kinematic
 324 experiment.

EMI-GPS referenced on	Directional error [m]		Median distance [m]		GNSS quality measures [m]		
	Longitude	Latitude	Reference	DGPS path	CEP	DRMS	DRMS2
Rover01 on DGPS	-0.79 ± 0.53	-0.90 ± 0.58	1.22	0.72	0.66	0.79	1.58
Rover02 on DGPS	-0.63 ± 0.32	-1.01 ± 0.98	1.34	0.60	0.79	1.03	2.05
Rover02 on Rover01	-0.17 ± 0.80	-0.05 ± 0.88	0.82	-	0.99	1.18	2.37

325





327

328 **Figure 5.** Comparison of the rotated and normalized EMI-GPS observations against the nearest RTK corrected DGPS
 329 location and against Rover01. The 2D accuracy of all EMI-GPS rover is quantified by the CEP, DRMS, and the 2DRMS in
 330 a – c). The dispersion of the standardized Rover observations taken in the NW-SE direction along the longest segment d-f)
 331 is compared against observations taken along the same segment on the return (g-i).

332

333

334

335

336

337

338

339

340

341

342

343

The median distance between the Rover observations and the DGPS reference location as well as towards the DGPS track was 1.22 m and 0.72 m for Rover01 and 1.34 m and 0.6 m for Rover02. The longitudinal error of Rover01 had a median of -0.79 m and a standard deviation of 0.53 m and was slightly larger than those of Rover02 (-0.63 ± 0.32 m). In contrast, a larger latitudinal error was obtained for Rover02 (-1.01 ± 0.98) than for Rover01 (-0.90 ± 0.58 m). The fact that observations of Rover01 were better circular distributed than those of Rover02 is reflected by the GNSS quality measures. For Rover01 a CEP of 0.66 m, a DRMS of 0.79 m, and a 2 DRMS of 1.58 m was obtained, while a CEP of 0.79 m, a DRMS of 1.03 m, and a 2DRMS of 2.05 m was calculated for Rover02. On the other hand, the normalisation of Rover02 on Rover01 indicated a more balanced distribution of the horizontal error between both Rovers. However, a CEP of 0.99 m, a DRMS of 1.18 m, and a 2DRMS of 2.37 m as well as a large standard deviation of the error ranging from 0.80 to 0.88 m suggests that both systems apparently obtained slightly different satellite information over time to calculate respective

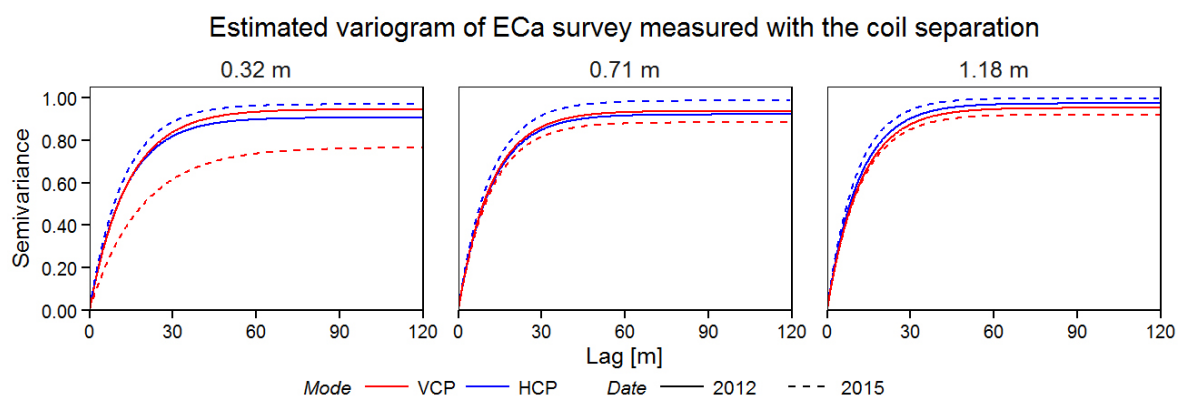
344 positions. Although, identical hardware components are used by the Rovers it can be assumed that the separation
 345 of Rover01 and Rover02 (see Figure 3a) by a multiple of the wavelength of the L1 frequency (~0.19 m) resulted
 346 in different multipath conditions and hence a different signal to noise ratio, which affected the system
 347 performance. Unfortunately, the recorded NMEA-GGA message does not provide further information and
 348 RAW messages were not recorded by the GNSS receivers.

349 The performance of both EMI-GPS receivers was further investigated along the longest segments of the
 350 test track. As illustrated in Figure 5d and e, the scattering of both Rovers indicates a similar position relative to
 351 the DGPS as the test chart was moved in the NW-SE direction. The apparent delay in the Rover positioning as
 352 suggested by the negative offset towards the DGPS can most likely be explained by the RTK-correction of the
 353 DGPS towards the south. This assumption is supported by Figure 5g and h which indicates a positive offset for
 354 most of the observations as the cart was pulled towards the opposite direction. Besides this, the comparison also
 355 indicates a more compact scattering of Rover02 compared to Rover01, especially on the return. This might
 356 explain the observed bi-modal distribution of the latitude error of Rover02. As summarised in Figure 5f and i
 357 deviations in the positioning between both systems occurred at any time with larger differences on the return.

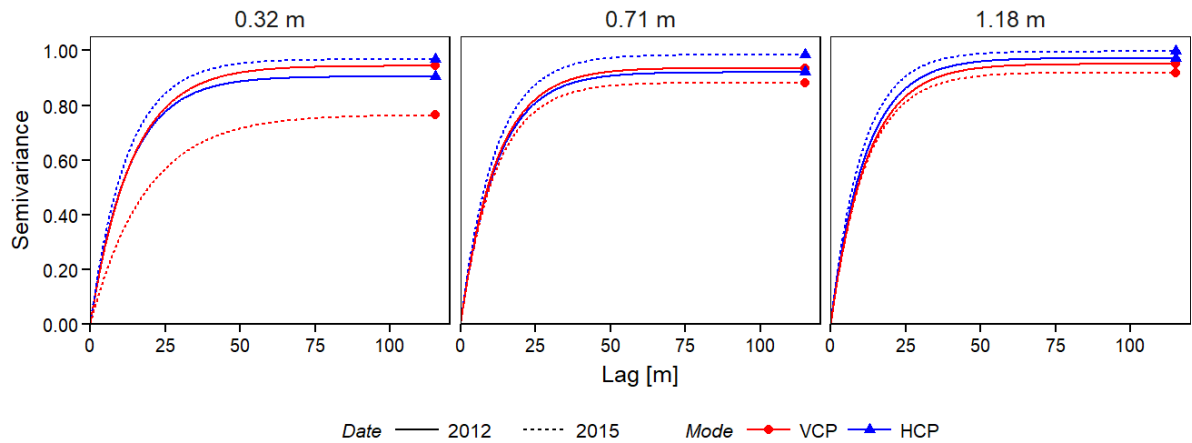
358 Although, the kinematic experiment indicated a relatively small absolute position error one should note
 359 that the number of observations is relatively small ($n = 1740$). Furthermore, a more robust experimental design
 360 with a longer baseline and a balanced change of directions as well as a high number of repetitions under different
 361 satellite constellations is needed to quantify the position accuracy of the EMI-GPS further.

362 *Quantification of the relative position accuracy of the EMI-GPS using EMI survey data*

363 As illustrated in Figure 6, the estimated variograms of the ECa measurements from the 2012 and 2015
 364 survey at the Selhausen site – field F01 -are remarkably similar. This is especially evident for the intermediate
 365 and deeper ECa data. Rudolph et al. (2015) showed that at this particular field, the clay content increased with
 366 depth. As the environmental conditions between the surveys were comparable, it is very likely that the spatial
 367 variability of the deeper measurements is controlled by the temporally stable clay content. The larger variation
 368 between the shallow VCP measurements can be related to the differences in the field management resulting in
 369 a different surface roughness and topsoil compaction (Brevik 2001).



370



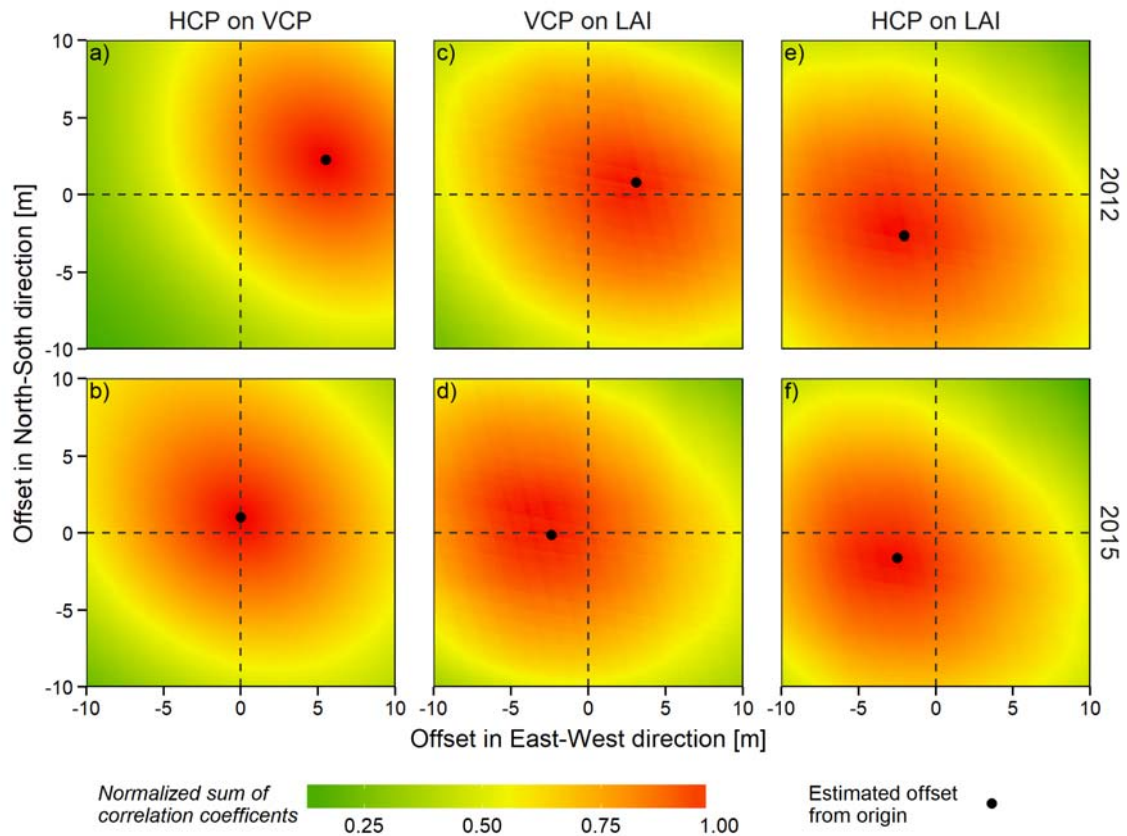
371

372 **Figure 6.** Comparison of the estimated spatial variability of the repeated 2012 and 2015 ECa survey at the TERENO test
 373 site Selhausen – field F01. Measurements were taken by the CMD miniExplorer in vertical coplanar (VCP) and horizontal
 374 coplanar (HCP) mode. The EMI sensor consists of three receiver coils separated by $d_1 = 0.32$, $d_2 = 0.71$, and $d_3 = 1.18$ m
 375 from the transmitter coil. The resulting theoretical exploration depth ranges from 0 - 0.25 m (VCP1), 0 - 0.5 m (VCP2), and
 376 0 - 0.9 m (VCP3) and from 0 - 0.5 m (HCP1), 0 - 1.1 m (HCP2) and 0 - 1.9 m (HCP3), respectively.

377 The Pearson correlation coefficients calculated between the measured VCP and HCP raster indicate a good
 378 correlation for the 2012 survey ranging from 0.67 to 0.70 and a very good correlation for the 2015 survey
 379 ranging from 0.80 to 0.93 (see Table 2). The low correlation between the shallow ECa measurements are most
 380 likely an artefact of the smaller footprint and sensing depth of the sensor. Also the higher sensitivity of the EMI
 381 mode towards environmental conditions should be considered.

382 The assumption that the lower correlations of the 2012 survey were attributed to positioning errors was
 383 investigated by estimating the relative position error between respective ECa measurements. Using the sum of
 384 correlations estimated from a predefined set of offset combinations as a criterion, the estimated error distribution
 385 is visualised in Figure 7 and quantified in Table 2. The analysis revealed an elliptic shaped pattern with high
 386 correlations near the origin and lower correlations further away. One should note that the origin represents the
 387 initial correlation of the measured data. The location with the highest sum of correlations instead defines the
 388 offset which should be applied to the measured HCP data to achieve the highest correlation towards VCP.
 389 Respectively, the estimated position offset quantifies the magnitude of the relative error and describes the
 390 corresponding replacement vector. Figure 7a illustrates that for the 2012 survey, the highest correspondence
 391 between VCP and HCP measurements was found when HCP measurements were shifted by 5.5 m towards the
 392 east. As a consequence, the correlation significantly improved to 0.89 and 0.92 respectively. In contrast, Figure
 393 7b illustrates the error distribution of the 2015 survey which suggests a relative error of only 1 m. As a
 394 consequence, only minor improvements were achieved, which do not show up in the summary statistics. As a
 395 consequence, the estimated error suggest that a tandem-approach, at which two EMI sensors were used
 396 simultaneously and geo-referenced individually, should be the preferred survey design as the effect of time-
 397 variable factors such as satellite constellation and atmospheric delay are minimal. However, multiple data sets
 398 from a variety of fields are needed to test this assumption further.

399



400

401 **Figure 7.** Comparison of the relative and absolute positioning error of the EMI-GPS receiver for two different survey designs. The relative position error was assessed by stepwise correlating the shifted VCP against HCP measurements while the absolute positioning error was obtained by correlating remotely sensed leaf area index measurements (LAI) against the shifted VCP and HCP data. For both approaches the sum of the estimated Pearson correlation coefficient was used to quantify the error and replacement vector to correct the ECa data.

406 *Quantification of the absolute positioning errors using remotely sensed LAI observations*

407 The initial correlation between the geo-referenced LAI raster image and the shallow VCP measurements
 408 of the 2012 survey ranged between 0.47 and 0.62 (see Table 3). A slightly higher correlation was calculated for
 409 respective HCP measurements ranging from 0.60 to 0.68. The correlation coefficients between LAI and the
 410 2015 ECa data were similar and ranged from 0.41 to 0.58. The determination and quantification of the absolute
 411 positioning error are visualised in Figure 7 c-f and summarised in Table 3. For the 2012 VCP measurements,
 412 the highest sum of correlation coefficients was determined by shifting the ECa raster by 3.2 m towards the east.
 413 In contrast, the highest correlation between LAI and HCP was located 3.35 m apart from the origin but in a
 414 westerly direction. The fact that both extrema were located in the opposite direction relative to the origin
 415 explains the previously determined large relative error. Although, a similar absolute position error was
 416 determined for the 2015 survey (2.4 and 3.0 m) the relative separation between both extrema was only 1 m.
 417 These findings are in good agreement with those made by the determination of the relative positioning error.
 418 The fact that the correlation between LAI and the position corrected ECa data improved only slightly, up to
 419 0.73 for 2012 and 0.62 for 2015, can partly be attributed to the low resolution of the LAI raster of 5 x 5 m as
 420 well as the magnitude of the absolute positioning error. Furthermore, one should note that firstly, ECa and LAI
 421 observations were made in different years while secondly the observed spatial variability of LAI is not

422 exclusively a function of soil texture. However, the assessment of the positioning error demonstrated that the
423 position accuracy of an EMI survey can be validated and improved using affordable comprehensive secondary
424 information. Certainly, the quantification of the positioning error of the EMI-GPS with a DGPS or self-tracking
425 total station (TTS) would be more precise, but expensive to realise especially if more than one EMI device has
426 to be geo-referenced.

427

428 **Table 2.** Comparison of the Pearson correlation coefficients obtained between measured and position corrected ECa data of the 2012 and 2015 EMI survey as well as quantification of the relative
 429 positioning errors and respective replacement vectors.

Survey date	Correction method	Pearson correlation coefficient between respective EMI measurements						Estimated replacement vector of the absolute positioning error			
		Original measured			Offset corrected			East-West offset [m]	North-South offset [m]	Angle [°]	Distance from optimum [m]
		HCP1 vs VCP2	HCP2 vs VCP2	HCP3 vs VCP3	HCP1 vs VCP2	HCP2 vs VCP2	HCP3 vs VCP3				
2012	VCP on HCP	0.67	0.69	0.70	0.89	0.90	0.92	5.50	2.25	22.25	5.94
2015	VCP on HCP	0.80	0.85	0.93	0.80	0.85	0.93	0.00	1.00	90.00	1.00

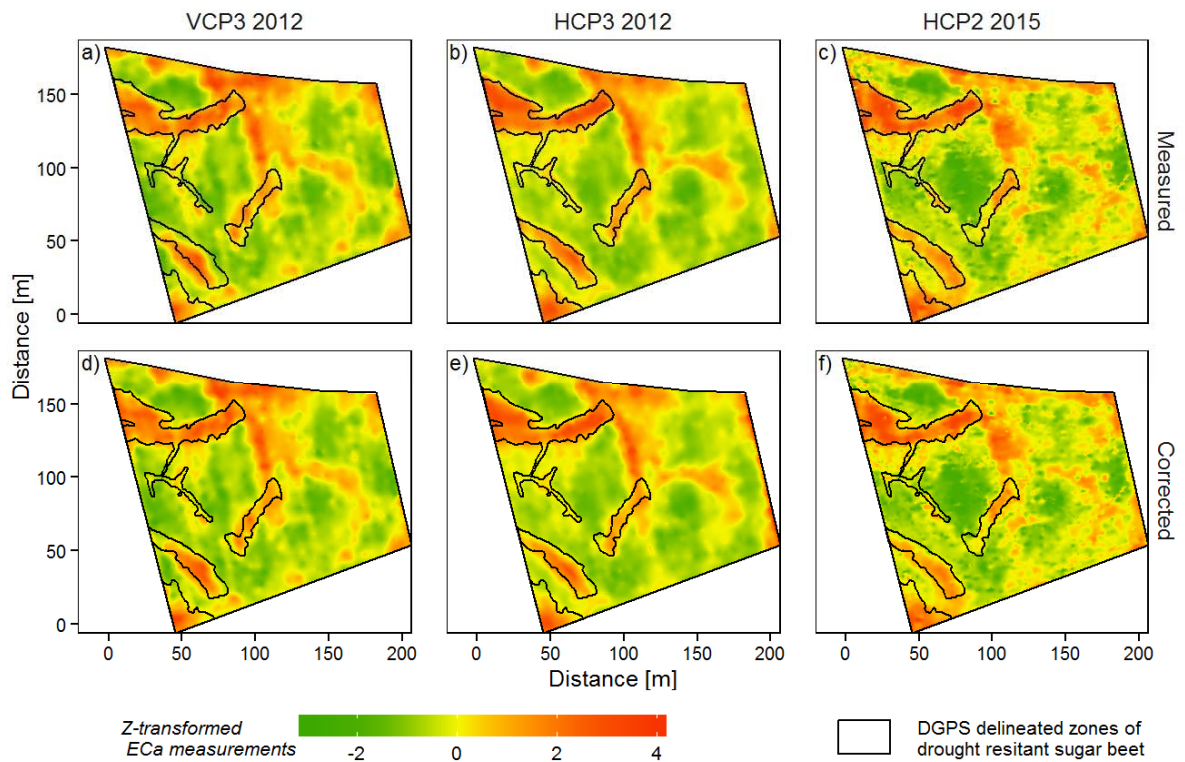
430
 431 **Table 3.** Comparison of the Pearson correlation coefficient obtained between remotely sensed leaf area index (LAI) image and the measured and position corrected ECa raster of the 2012 and 2015
 432 EMI survey as well as the quantification of the absolute positioning errors and respective replacement vectors.

Survey date	Correction method	Pearson correlation coefficient between respective EMI measurements						Estimated replacement vector of the absolute positioning error			
		Original measured			Offset corrected			East-West offset [m]	North-South offset [m]	Angle [°]	Distance from optimum [m]
		HCP1 vs VCP2	HCP2 vs VCP2	HCP3 vs VCP3	HCP1 vs VCP2	HCP2 vs VCP2	HCP3 vs VCP3				
24.07.2012	VCP on LAI	0.47	0.61	0.62	0.50	0.64	0.66	3.10	0.80	14.47	3.20
25.07.2012	HCP on LAI	0.60	0.66	0.68	0.65	0.70	0.73	-2.30	-2.35	-45.6	3.29
19.08.2015	VCP on LAI	0.41	0.56	0.58	0.44	0.59	0.61	-2.40	-0.15	-3.5763	2.40
19.08.2015	HCP on LAI	0.46	0.51	0.58	0.49	0.55	0.62	-2.50	-1.65	-33.424	3.00

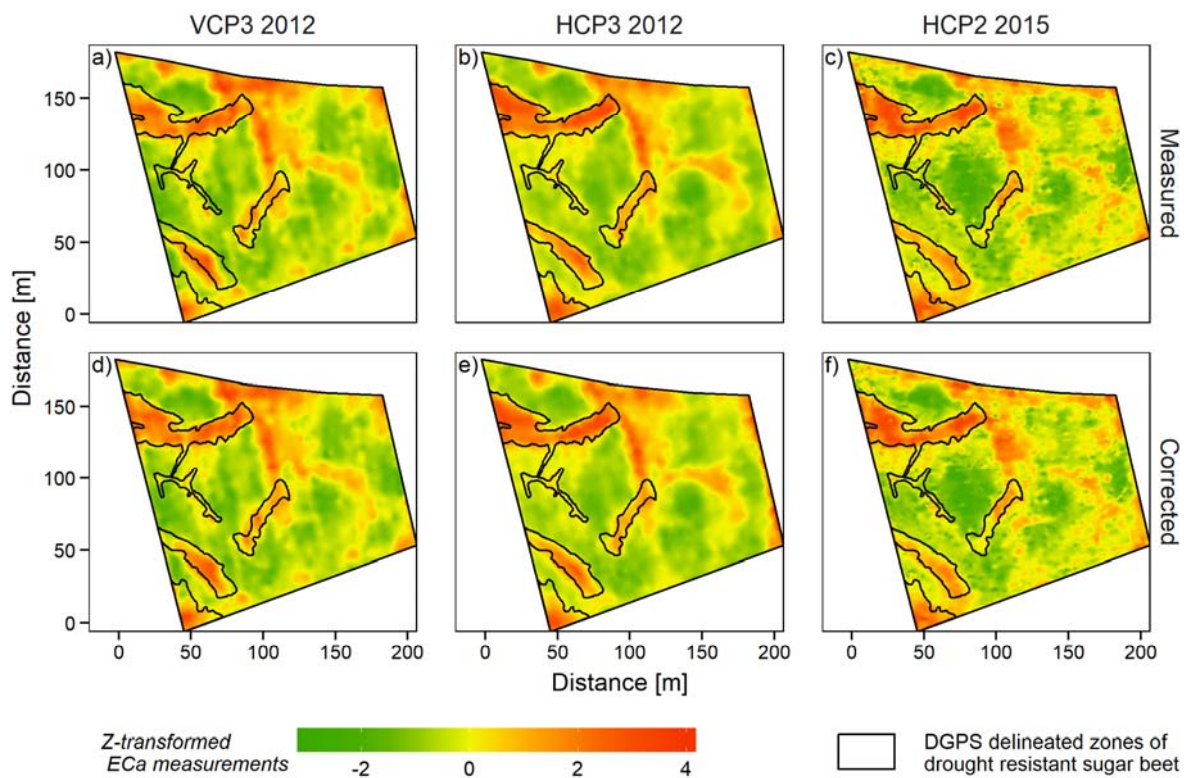
433

434 *Validation of the position corrected ECa data using independent secondary information*

435 The comparison between the DGPS delineated zones of non-drought affected sugar beet as observed in
436 2013 and described by Rudolph et al. (2015) against the measured and position corrected ECa data normalised
437 on its mean and standard deviation are depicted in Figure 8. The non-drought affected zones are well described
438 by higher ECa values due to the high clay content in the subsoil. However, as indicated in Figure 8a-c slight
439 deviations, especially for the first zone from the north as well as for the second zone from the south are obvious.
440 While respective VCP measurements appear to be shifted towards the south-west the deeper HCP measurements
441 tend to be positioned too far north. Although, these discrepancies can be of natural origin, ECa patterns almost
442 align perfectly after the position was corrected using the geo-referenced LAI image raster (see Figure 8d-f).



443



444

445 Figure 8. Comparison between the interpolated measured and position corrected ECa data against DGPS delineated zones
 446 of drought affected sugar beet.

447 To evaluate the correction of the absolute positioning error further, soil texture information obtained and
 448 described by Rudolph et al. (2015) were regressed against ECa. The coefficients of determination are compared
 449 in Table 4. Considerable improvements were found against topsoil texture for the 2015 ECa survey as well as
 450 the 2012 HCP measurements. In contrast, the position correction of the 2012 VCP measurements only slightly
 451 improved the prediction of subsoil clay content. Please note that the soil sampling campaign was directed by
 452 the LAI observations with the purpose of describing the transition in soil parent material within the narrow and
 453 undulating patterns. It is, therefore, understandable that the regression between ECa and soil texture improved
 454 as the position of ECa was corrected on LAI. In contrast, no or only minor improvements should have been
 455 expected if soil samples would have been taken within the homogeneous parts of the field.

456

457 **Table 4.** Comparison of the coefficients of determination (R^2) calculated between soil texture and the measured and position
 458 corrected ECa of the 2012 and 2015 EMI survey.

Survey date	EMI mode	Coefficient of determination (R^2)									
		Gravel		Sand topsoil		Silt topsoil		Clay topsoil		Clay subsoil	
		Before	After	Before	After	Before	After	Before	After	Before	After
2012	VCP1	0.43	0.40	0.14	0.10	0.32	0.20	0.23	0.18	0.23	0.24
	VCP2	0.53	0.50	0.26	0.20	0.40	0.28	0.31	0.28	0.53	0.54
	VCP3	0.53	0.51	0.32	0.25	0.42	0.31	0.34	0.29	0.59	0.65
	HCP1	0.32	0.50	0.07	0.16	0.14	0.30	0.21	0.32	0.33	0.34
	HCP2	0.34	0.54	0.13	0.25	0.13	0.33	0.25	0.35	0.62	0.57
	HCP3	0.39	0.54	0.16	0.27	0.16	0.33	0.27	0.33	0.68	0.65
2015	VCP1	0.19	0.11	0.01	0.00	0.04	0.01	0.08	0.07	0.09	0.02
	VCP2	0.32	0.40	0.05	0.10	0.07	0.14	0.17	0.33	0.19	0.25
	VCP3	0.40	0.52	0.12	0.20	0.13	0.24	0.23	0.34	0.46	0.40
	HCP1	0.37	0.45	0.11	0.21	0.09	0.19	0.30	0.33	0.40	0.37
	HCP2	0.36	0.53	0.13	0.23	0.08	0.23	0.29	0.36	0.45	0.47
	HCP3	0.40	0.54	0.17	0.31	0.13	0.29	0.29	0.36	0.61	0.56

459 **Practical implications for the geo-referencing of ECa data using GNSS sensors**

460 Based on the experiments conducted in this study using a DGPS and EMI-GPS the following practical
 461 implications should be considered for future EMI-surveys geo-referenced by any GNSS receiver.

462 First, the position accuracy of geodetic-grade DGPS receivers with RTK-correction is remarkably precise.
 463 However, most PA applications are carried out at remote locations where a reliable and stable GSM connection
 464 cannot be guaranteed. As an alternative, RTK corrections from a second nearby DGPS system can be used to
 465 precisely collect position information. However, the so-called base and rover configuration requires that the
 466 coordinates of the base station are known to obtain absolute measurements. Moreover, the loss of the RTK
 467 correction will introduce positioning errors which are difficult to correct using professional and costly post-
 468 processing software. Although, such erroneous observations can also be removed, one should consider that,
 469 depending on the survey speed, parts of the survey area will remain unsampled. Such gaps will irretrievably
 470 introduce uncertainty into the spatial estimation and interpolation of the property of interest.

471 Another factor which should be considered when using DGPS is a delay due to the latency of the DGPS.
 472 This is the time that a receiver needs to calculate and output the position, but also due to time lags in the data
 473 acquisition system (Sudduth et al. 2001). Both time lags will convert to a distance error depending on the speed
 474 of motion. Ehrl et al. (2003) showed that a DGPS has a considerably longer latency than a low-cost receiver
 475 due to the use of complex algorithms to determine its position. However, Lark et al. (1997) demonstrated that
 476 the delay can be estimated and corrected by minimizing the mean squared difference calculated between
 477 neighboring observations from adjacent passes and for a set of pre-defined offsets.

478 Second, SBAS corrected GNSS observations with an absolute positioning error of 2 m are sufficient for
 479 most PA applications. However, to guarantee optimal GNSS performance, the quality of the GNSS antenna as

480 well as its positioning is crucial. Large performance differences mainly due to a less effective signal reception
481 and multipath suppression have been reported between geodetic-grade and consumer-grade patch antennas
482 (Takasu and Yasuda 2008; Pesyna et al. 2014; Odolinski and Teunissen 2016). To improve the signal quality
483 one should first ensure that the antenna matches the technology of the GNSS receiver (Matias et al. 2015). Then,
484 the antenna should be placed on a ground plane, such as a conductive plate, to reduce multipath and mounted
485 at least 1.5 m above ground, apart from any electronic device to minimize radio-frequency interference.
486 Furthermore, a cut-off angle of at least 15° is advisable but should be increased if required (Odolinski and
487 Teunissen 2016). Moreover, the performance of the GNSS system should be at least once compared against a
488 precise reference system such as a RTK-DGPS or TTS using stationary and dynamic measurements (Ehrl et al.
489 2003). If several GNSS positioning modules or antennas are available a sensitive test, in which the GNSS
490 configuration to be tested is compared against a reference, should be considered to evaluate the best performing
491 unit or configuration (Takasu and Yasuda 2008; Pesyna et al. 2014). Commonly used quality control parameters
492 are the carrier-to-noise density or the signal-to-noise ratio (Kaplan and Hegarty 2006).

493 Third, when considering SBAS correction only, it is highly recommended to design the EMI survey
494 carefully. As better accuracy is achieved along straight transects, measurements should be primarily carried out
495 along evenly spaced transects, whereas the distance between them should be optimised regarding the expected
496 accuracy of the GNSS receiver and the size of the survey area. Turning points instead should be located in the
497 headland area or beyond field boundaries and survey interruption should be minimised if possible.

498 Fourth, if the purpose of the survey is to obtain ECa measurements from different depths by either using
499 several EMI modes or several EMI device, one has to ensure that the measurements are taken over a relatively
500 short time period to minimise factors such as satellite constellation and atmospheric delay. Note, that the satellite
501 constellation for a given area can be predicted using freely available software such as the Trimble Planning
502 Software (Trimble, Sunnyvale, USA). However, EMI devices which are capable of obtaining measurements
503 from several depths without repeating the survey such as the EM-38DD or the Dual-EM's are perfectly suited.
504 In contrast, the combination of several sensors to the so-called tandem-approach has been presented as a
505 promising alternative.

506 Fifth, to minimise interference between the GNSS and EMI unit (von Hebel et al. 2014) a number of
507 published studies obtained position information from a DGPS placed with a spatial offset in front of the EMI
508 sensor. Under the assumption that the sensor had followed in a straight line and at a constant distance the offset
509 was corrected using sophisticated post-processing (see e.g. Sudduth et al. (2001); Gottfried et al. (2012);
510 Delefortrie et al. (2014)). As a spatial offset adds uncertainty to the geostatistical estimation of the measured
511 variable (Cressie and Kornak 2003), the use of a compact GNSS system centred above the EMI sensor within
512 appropriate height is recommended.

513 Finally, even if position errors are apparent, respective measurements can be corrected using
514 comprehensive secondary information, which can be related to the response variable. As an alternative, geo-
515 referenced tracks collected along distinct features such as field boundaries or tram lines can be compared against
516 remotely sensed images to quantify and correct respective measurements. However, one should note that the
517 estimated position error will be variable between surveys if no RTK correction is used.

518

519 **Conclusion**

520 In this study, an affordable, single-frequency GPS system developed for EMI surveys supporting PA
521 applications was introduced. Comparisons between the EMI-GPS and a RTK-DGPS with centimetre accuracy
522 indicated that the averaged absolute position error never exceeded 1.5 m. While the DGPS occasionally suffered
523 from weak RTK correction no erratic behaviour was evident for the EMI-GPS. ECa survey data indicates a
524 good accuracy of the EMI-GPS along straight transects with a higher variation in the positioning at turning
525 points or at fixed locations. Moreover, ECa data suggests that the absolute positioning error of the EMI-GPS
526 remained constant over the period of a survey but varied between surveys. Furthermore, data indicates that the
527 relative positioning error was larger when measurements were obtained on different dates. To minimise the
528 effects of time variable factors such as satellite constellation and atmospheric delay the concurrent measurement
529 of both shallow and deep EMI modes is proposed. Finally, geo-referenced ECa data suggest that for most PA
530 applications the low-cost, single-frequency EMI-GPS is a promising alternative to the expensive geodetic-grade
531 RTK-DGPS systems.
532

533 **Conflicts of interest:** The authors declare no conflict of interest.

534 **References**

535

536

537 Bogena, H., Borg, E., Brauer, A., Dietrich, P., Hajnsek, I., Heinrich, I., et al. (2016). TERENO: German
538 network of terrestrial environmental observatories. *Journal of large-scale research facilities*,
539 2(A52).

540 Bramley, R. G. V. (2009). Lessons from nearly 20 years of Precision Agriculture research,
541 development, and adoption as a guide to its appropriate application. *Crop & Pasture*
542 *Science*, 60(3), 197-217.

543 Brevik, E. C. (2001). *Evaluation of selected factors that may influence the application of*
544 *electromagnetic induction technology to soil science investigation in Iowa*. Iowa State
545 University, Ames, Iowa.

546 Corwin, D. L. (2008). Past, present, and future trends of soil electrical conductivity measurements
547 using geophysical methods. In B. Allred, J. J. Daniels, & M. R. Ehsani (Eds.), *Handbook of*
548 *Agricultural Geophysics* (pp. 17-44): CRC Press.

549 Cressie, N., & Kornak, J. (2003). Spatial statistics in the presence of location error with an application
550 to remote sensing of the environment. *Statistical Science*, 18(4), 436-456.

551 Delefortrie, S., De Smedt, P., Saey, T., Van De Vijver, E., & Van Meirvenne, M. (2014). An efficient
552 calibration procedure for correction of drift in EMI survey data. *Journal of Applied*
553 *Geophysics*, 110, 115-125.

554 Ehrl, M., Stempfhuber, W., Auernhammer, H., & Demmel, M. Quality assessment of agricultural
555 positioning and communication systems. In J. V. Stafford, & A. Werner (Eds.), *Precision*
556 *agriculture: Proceedings of the 4th European Conference on Precision Agriculture, Berlin,*
557 *15-19 June 2003* (pp. 205-210): The Netherlands: Wageningen Academic Publishers

558 Eigenberg, R. A., & Nienaber, J. A. (2003). Electromagnetic induction methods applied to an
559 abandoned manure handling site to determine nutrient buildup. *Journal of Environmental*
560 *Quality*, 32, 1837-1843.

561 El-Rabbany, A. (2006). *Introduction to GPS: The Global Positioning System* (Vol. 2). Massachusetts,
562 United States: Artech House.

563 Francés, A. P., & Lubczynski, M. W. (2011). Topsoil thickness prediction at the catchment scale by
564 integration of invasive sampling, surface geophysics, remote sensing and statistical
565 modeling. *Journal of Hydrology*, 405, 31-47.

566 Frogbrook, Z. L., & Oliver, M. A. (2007). Identifying management zones in agricultural fields using
567 spatially constrained classification of soil and ancillary data. *Soil Use and Management*, 23,
568 40-51.

569 Gottfried, T., Auerswald, K., & Ostler, U. (2012). Kinematic correction for a spatial offset between
570 sensor and position data in on-the-go sensor applications. *Computers and Electronics in*
571 *Agriculture*, 84, 76-84.

572 Huang, J., Nhan, T., Wong, V. N. L., Johnston, S. G., Lark, R. M., & Triantafilis, J. (2014). Digital soil
573 mapping of a coastal acid sulfate soil landscape. *Soil Research*, 52(4), 327-339.

574 Jaynes, D. B., Colvin, T. S., & Ambuel, J. Yield mapping by electromagnetic induction. In P. C. Robert,
575 R. H. Rust, & W. E. Larson (Eds.), *Proceedings of the Second International Conference on*

576 *Precision Agriculture. Madison, WI, USA, Minneapolis, 1995* (pp. 383-394). no: ASA-CSSA-
577 SSA

578 Kachanoski, R. G., Gregorisch, E. G., & van Wesenbeeck, I. J. (1988). Estimating spatial variations of
579 soil water content using noncontacting electromagnetic inductive methods. *Canadian*
580 *Journal of Soil Science, 68*, 715-722.

581 Kaplan, E. D., & Hegarty, C. J. (2006). *Understanding GPS - Principles and Applications* (2ed.).
582 Massachusetts, United States: Artech House.

583 Kobayashi, M., Ingels, F., & Bennett, G. (1992). *Determination of the probability density function of*
584 *GPS (Global Positioning Systems) positioning error*. Paper presented at the Proceedings of
585 the 48th annual meeting of the institute of navigation, Dayton,

586 Lark, R. M., Stafford, J. V., & Bolam, H. C. (1997). Limitations on the spatial resolution of yield
587 mapping for combinable crops. *Journal of Agricultural Engineering Research, 66*(3), 183-193.

588 Leick, A., Rapoport, L., & Tatarnikov, D. (2015). *GPS satellite surveying* (Fourth edition. ed.). New
589 Jersey, USA: Wiley.

590 López-Lozano, R., Casterad, M. A., & Herrero, J. (2010). Site-specific management units in a
591 commercial maize plot delineated using very high resolution remote sensing and soil
592 properties mapping. *Computers and Electronics in Agriculture, 73*, 219-229.

593 Matérn, B. (1986). *Spatial Variation* (Vol. 36, Lecture Notes in Statistics). New York, USA: Springer.

594 Matias, B., Oliveira, H., Almeida, J., Dias, A., Ferreira, H., Martins, A., et al. High-accuracy low-cost
595 RTK-GPS for an unmanned surface vehicle. In *OCEANS 2015, Genova, Italy 18-21 May*
596 *2015 2015* (pp. 1-4): IEEE

597 McBratney, A. B., & Pringle, M. J. (1999). Estimating average and proportional variograms of soil
598 properties and their potential use in Precision Agriculture. *Precision Agriculture, 1*(2), 125-
599 152.

600 McBratney, A. B., Santos, M. L. M., & Minasny, B. (2003). On digital soil mapping. *Geoderma, 117*(1-
601 2), 3-52.

602 McCloud, P. R., Gronwald, R., & Kuykendall, H. (2007). Precision agriculture: NRCS support for
603 emerging technologies. Agronomy Technical Note No.1. Washington, USA.

604 Mertens, F. M., Pätzold, S., & Welp, G. (2008). Spatial heterogeneity of soil properties and its
605 mapping with apparent electrical conductivity. *Journal of Plant Nutrition and Soil Science,*
606 *171*, 146-154.

607 Minasny, B., & McBratney, A. B. (2005). The Matern function as a general model for soil variograms.
608 *Geoderma, 128*(3-4), 192-207.

609 National Marine Electronics Association (2012). NMEA 0183, The Standard for Interfacing Marine
610 Electronics. New Bern, USA: www.nmea.org.

611 NovAtel Inc. (2003). GPS Position Accuracy Measures. APN-029 Rev 1. Calgary, Canada.

612 O’Leary, G. (2006). Standards for electromagnetic induction mapping in the grains industry. In J.
613 Peters (Ed.), *GRDC Precision Agriculture Manual* Barton, Australia: Grains research and
614 development corporation.

615 Odolinski, R., & Teunissen, P. J. G. (2016). Single-frequency, dual-GNSS versus dual-frequency,
616 single-GNSS: a low-cost and high-grade receivers GPS-BDS RTK analysis. *Journal of Geodesy,*
617 *90*(11), 1255-1278.

618 Pesyna, K. M. J., Heath, R. W. J., & Humphreys, T. E. Centimeter positioning with a smartphone-
619 quality GNSS Antenna. In *27th international technical meeting of the satellite division of*
620 *the Institute of Navigation, Tampa, USA, 2014* (pp. 1568-1577): ION Publications

621 Rudolph, S., van der Kruk, J., von Hebel, C., Ali, M., Herbst, M., Montzka, C., et al. (2015). Linking
622 satellite derived LAI patterns with subsoil heterogeneity using large-scale ground-based
623 electromagnetic induction measurements. *Geoderma*, 241-242, 262-271.

624 Rudolph, S., Wonglecharoen, C., Lark, R. M., Marchant, B. P., Garré, S., Herbst, M., et al. (2016).
625 Soil apparent conductivity measurements for planning and analysis of agricultural
626 experiments: A case study from Western-Thailand. *Geoderma*, 267, 220-229.

627 Sudduth, K. A., Drummond, S. T., & Kitchen, N. R. (2001). Accuracy issues in electromagnetic
628 induction sensing of soil electrical conductivity for precision agriculture. *Computers and*
629 *Electronics in Agriculture*, 31(3), 239-264.

630 Takasu, T., & Yasuda, A. Evaluation of RTK-GPS performance with low-cost single-frequency GPS
631 receivers. In *International symposium on GPS/GNSS 2008, Tokyo, Japan, 2008* (pp. 852-
632 861)

633 Takasu, T., & Yasuda, A. Development of the low-cost RTK-GPS receiver with an open source
634 program package RTKLIB. In *International Symposium on GPS/GNSS, Jeju, Korea, 2009* (pp.
635 4-6)

636 Taylor, R. K., Schrock, M. D., Bloomfield, J., Bora, G., Brockmeier, G., Burton, W., et al. (2004).
637 Dynamic testing of GPS receivers. *Transactions of the ASAE*, 47(4), 1017-1025.

638 Triantafilis, J., & Lesch, S. M. (2005). Mapping clay content variation using electromagnetic induction
639 techniques. *Computers and Electronics in Agriculture*, 46(1-3), 203-237.

640 Ublox (2010). LEA-6 u-blox 6 GPS modules data sheet. Thalwil, Swiss.

641 Ublox (2016). U-center: GNSS evaluation software for Windows. Thalwil, Swiss.

642 Vitharana, U. W. A., van Meirvenne, M., Simpson, D., Cockx, L., & de Baerdemaeker, J. (2008). Key
643 soil and topographic properties to delineate potential management classes for precision
644 agriculture in the European loess area. *Geoderma*, 143, 206-215.

645 von Hebel, C., Rudolph, S., Mester, A., Huisman, J. A., Kumbhar, P., Vereecken, H., et al. (2014).
646 Three-dimensional imaging of subsurface structural patterns using quantitative large-scale
647 multiconfiguration electromagnetic induction data. *Water Resources Research*, 50(3), 2732-
648 2748, doi:10.1002/2013wr014864.

649 Webster, R., & Oliver, M. A. (2007). *Geostatistics for environmental scientists*. Chichester, UK: John
650 Wiley & Sons Ltd.

651 Weltzien, C., Noack, P. O., & Persdson, K. GPS receiver accuracy test - dynamic and static for best
652 comparison of results. In J. Stafford, & A. Werner (Eds.), *Proceedings of the 4th European*
653 *Conference on Precision Agriculture, Berlin, 2003* (pp. 717-722): The Netherlands:
654 Wageningen Academic Publishers
655